Nuclear Instruments and Methods in Physics Research B 404 (2017) 52–57

Contents lists available at ScienceDirect

Nuclear Instruments and Methods in Physics Research B

journal homepage: www.elsevier.com/locate/nimb

Performance test of high brightness nano-aperture ion source

Xinxin Xu [a], P. Santhana Raman [a,b], Rudy Pang [a,b], Nannan Liu [a], Anjam Khursheed [b], Jeroen A. van Kan [a,*]

[a] Centre for Ion Beam Applications, Department of Physics, National University of Singapore, Singapore 117542, Singapore
[b] Department of Electrical and Computer Engineering, National University of Singapore, Singapore 117583 Singapore

ARTICLE INFO

Article history:
Received 2 September 2016
Received in revised form 5 November 2016
Accepted 23 January 2017
Available online 4 February 2017

Keywords:
Proton beam writing
Nano-aperture ion source
High brightness

ABSTRACT

The nano-aperture ion source (NAIS) is a candidate to be part of a compact proton beam writing system, which has the potential of high throughput with sub 10 nm spot sizes. To evaluate the performance of this ion source, different NAIS chip configurations were examined through simulation. This study suggests that a proton reduced brightness of more than 10^6 A/(m^{2}srV) can be achieved, with an ion energy spread of less than 1 eV. Meanwhile, a prototype NAIS has been fabricated and tested to deliver 800 A/(m^{2}srV) of reduced brightness for Ar^+ beam. Current limitations and further improvements of this prototype NAIS are discussed.

© 2017 Elsevier B.V. All rights reserved.

1. Introduction

Proton beam writing (PBW) is a promising candidate as a next-generation lithographic technique with the capability to fabricate high aspect ratio nano-structures [1–10]. Compared with electron beam lithography (EBL), focused MeV protons deliver a straighter and deeper energy deposition in materials. A minimal proximity effect is observed in structures because of limited energy transfer from incoming protons to substrate's secondary electrons, due to their mass mismatch [11,12]. Based on these prime features, PBW has been employed in many research areas like photonics, microfluidic devices, nano-imprinting, and material modification [2,13]. Currently, the smallest structures written by PBW are 19 nm lines in 100 nm thick hydrogen silsesquioxane [14]. A 9.3×32 nm^2 proton beam spot size has been achieved at Centre for Ion Beam Applications (CIBA), National University of Singapore [15]. But currently, the low brightness radio frequency (RF) ion source (20–30 A/(m^{2}srV)) [16,17] restricts the beam resolution and throughput in PBW. People are developing alternative high brightness ion sources following different strategies [18–20]. According to our knowledge high brightness proton sources (>10^4 A/(m^{2}srV)) have not been reported. To further improve the performance of PBW, a high brightness nano-aperture ion source (NAIS) [21–24] is under development in CIBA. The aim of this ion source is to improve the beam brightness through source size reduction down to 100 nm with a sub-micron ionization chamber, as shown in Fig. 1.

2. Simulation of NAIS configurations

The concept of NAIS is to ionize gas that is present in the sub-micron ionization chamber through high energy electrons, as shown in Fig. 1. The beam parameters for an ideal NAIS performance have been simulated and evaluated as explained in the following steps. First, the gas distribution (in the sub-micron ionization chamber) is analyzed using COMSOL Multiphysics® [25], a finite element analysis software (see Fig. 2). The gas distribution and injected electron distribution determine the ion beam emission profile. Second, Poisson Superfish [26] is applied to calculate the electric field generated in z-axial symmetric cylindrical coordinates. Results from these simulations are fed into General Particle Tracer (GPT) package [27], to simulate beam trajectories and beam emittance from the NAIS. The injected electron energy is fixed at 1 keV as a trade-off between the ionization cross section and practical performances of available electron guns [21]. The extractor plate is biased to – 1 kV and is placed 1 mm away from NAIS, so as to extract the ion beam and at the same time prevent the injected electrons from entering the downstream of the setup.

2.1. Simulation of gas distribution in the NAIS

Inside the NAIS ionization chamber, ions are not generated from a single point or plane but originate from a sub-micrometer volume. Since the ionization probability is directly dependent on the availability of gas molecules, it is important to identify the gas distribution inside the ionization region. Knowing the spatial distribution, where individual ions are generated, will provide information about initial energy spread of the proton beam originating from the

* Corresponding author.
E-mail address: phyjavk@nus.edu.sg (J.A. van Kan).

http://dx.doi.org/10.1016/j.nimb.2017.01.051
0168-583X/© 2017 Elsevier B.V. All rights reserved.

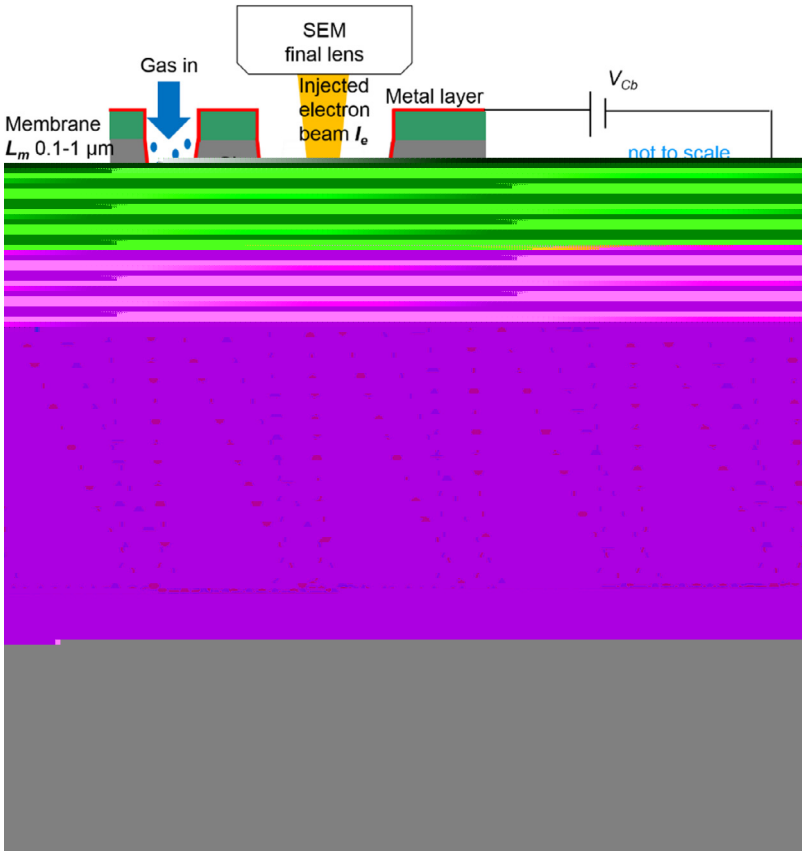

Fig. 1. Schematic setup of NAIS and the brightness measurement.

Fig. 2. Hydrogen gas pressure contour (simulated by COMSOL) for 100 nm spacer, 100 nm membranes, and 100 nm double-aperture configuration at 1000 mbar inlet gas pressure.

NAIS. To simplify the simulation, the gas distribution is considered to be cylindrically symmetric along the z-axis. The electric field inside the ionization chamber is fixed at 10^7 V/m. The choice of this value is a trade-off between reduced Coulomb effect and minimal energy spread. The input pressure of hydrogen gas is assumed to be 1000 mbar at room temperature (~300 K) and is in the laminar flow regime. In the spacer, the gas density reduces from the gas inlet to the centre of the chip (see Fig. 2). While the injected electron current density is taken to be a Gaussian distribution [28], we calculated that the generated proton beam is quasi-uniformly distributed in the radial plane of NAIS. Considering that the electron beam along the z-axis is continuous and uniform, the generated

can only extract part of the protons (~50%), resulting in an extracted proton beam current of ~250 pA. The remaining protons escape from the NAIS entrance aperture and/or collide with the membrane walls. This collision effect reduces the proton beam current and consequently lowers the beam emittance. From the proton beam trajectory (Fig. 5), we can notice that the double-aperture configuration also acts as a focusing lens which limits the divergence of the initial proton beam.

The brightness is derived from emittance and is given as [30],

$$B_r = \frac{2I}{\pi^2 \epsilon^2} = \frac{2I}{16\pi^2 \epsilon_{rms}^2} \quad (1)$$

where I is the total beam current, and ϵ is the edge emittance along radial plane, ϵ_{rms} is the root mean square (rms) emittance.

On substituting the values obtained from GPT simulations into Eq. (1), for 100% of extracted protons, the reduced brightness is calculated to be 1.4×10^5 A/(m^{2}srV), which is 4 orders larger than the existing PBW system [17]. In order to obtain higher brightness, 50% of the proton beam can be collimated, resulting in a reduced brightness as high as 1.5×10^6 A/(m^{2}srV).

In the above simulation, the incoming electron beam covers the entire area of the double-aperture. This can cause clogging of the double-aperture. To prevent this effect, the injected electron beam is illuminating half the diameter of the double-aperture, in the GPT simulation. The corresponding proton beam trajectories are shown in Fig. 5. In this case, due to the extra distance between the generated proton beam and membrane walls, fewer protons collide with the ionization chamber, therefore a higher percentage of the generated proton beam can be extracted (63%, with a current of ~80 pA). However, this increased extracted beam will contain a higher fraction of high-angled scattered protons, resulting in a small increase of beam emittance (~7% when compared to the case discussed in the preceding paragraph). For all the extracted protons, the reduced brightness is 4×10^4 A/(m^{2}srV) and for 50% of the collimated proton beam, the reduced brightness is 4×10^5 A/(m^{2}srV). It is obvious that reducing the injected electron beam size results in a significant decrease in beam current and a slight increase in beam emittance, giving a lower reduced brightness. The value of electron beam diameter is thus chosen such that there is a trade-off between the competing effects of higher ion B_r output and double-aperture clogging. Hence a preferred electron beam size would be slightly smaller than the double-aperture size without lowering the beam brightness significantly.

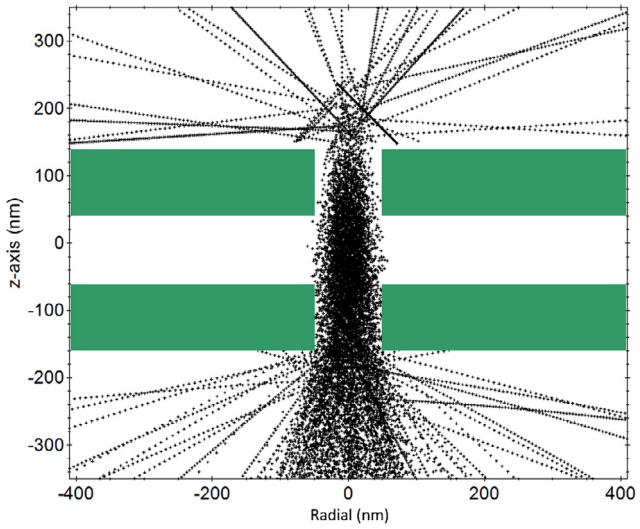

Fig. 5. Proton beam trajectory (simulated by GPT), the injected electron beam (used a Schottky emitter with 2×10^8 A/m^2 current density) covers half diameter of the double-aperture at the preferred configuration (La = 100 nm, Ls = 100 nm, and Lm = 100 nm at an axial gas pressure of 1000 mbar).

Space charge effect, inside the NAIS ionization volume, is an important parameter to be considered, which limits the maximum current density located across these parallel electrodes, as given by Child-Langmuir law [31,32]. For 2D Child-Langmuir Law [33], the maximum current density $J(2)$ is given by,

$$J(2) \cong J(1)\left(1 + \frac{D}{\pi L_a}\right) = \frac{4\varepsilon_0}{9D^2}\left(\frac{2e}{m}\right)^{1/2} V^{3/2}\left(1 + \frac{D}{\pi L_a}\right) \quad (2)$$

where $J(1)$ is the maximum current density in 1D model, D is the separation between electrodes (300 nm), V is the chip bias (3 V), e and m are the charge and mass of ion, respectively, ε_0 is the permittivity of free space, and L_a is the emitting width of the source.

Considering the fact that both proton (5.6%) and H_2^+ (94.4%) are generated simultaneously inside the ionization volume from hydrogen gas, the maximum H_2^+ current density is 1.2×10^6 A/m^2 in this simulated scenario. From Eq. (2), the maximum current density $J(2)$ for this preferred configuration is 4.4×10^6 A/m^2. This maximum current density is greater than in the simulated scenario, which means the operating-regime of NAIS is below the Child-Langmuir's limit. Furthermore, this maximum current density from Eq. (2) is derived from the situation where all ions are generated from one electrode plane. In NAIS, ions are generated in the entire volume of the ionization chamber resulting in a further reduction of space charge effect. Even more important, in NAIS, is that the injected electrons have the ability to compensate the space charge effect. Therefore, it is reasonable to neglect the space charge effect here.

3. Experimental result from the prototype NAIS

From an experimental perspective, the reduced brightness is given by [34,35],

$$B_r = \frac{I_a}{A_s \Omega V_{Ext}} = \frac{I_a}{A_s \frac{A_a}{L^2} V_{Ext}} \quad (3)$$

where I_a is the axial ion current, A_s is the virtual source area, Ω is the solid angle of the ion beam, V_{Ext} is the extracted ion beam potential, A_a is the area of the angular aperture's opening, and L is the distance from ionization chamber to the angular aperture.

An experiment for measuring source reduced brightness was performed (as shown in Fig. 1) inside a SEM (Philips XL 30 field emission) chamber. The SEM was employed to inject focused electron beam into the ionization chamber. The extractor was biased at a negative potential V_{ext}, serving two purposes: to deflect the injected electrons and to accelerate the ion beam. An angular aperture with an opening of 100 μm × 100 μm was positioned 10 mm away from the ionization chamber, which is mounted on a piezo-XY linear positioner. This angular aperture was precisely controlled to obtain maximum axial ion beam current. After the angular aperture, a suppressor was biased at the same potential as the extractor to maintain a uniform field and suppress the secondary electrons when ions land in the Faraday cup. The Faraday cup was biased at −36 V, to supply a landing potential for the ions. The NAIS ionization chamber and angular apertures were fabricated using MEMS technology [23]. The dimensions of the current prototype NAIS ionization chamber is as follows: membrane thickness (L_m) = 1 μm, double-aperture size (L_a) = 1.3 μm, and spacer thickness (L_s) = 500 nm. The injected electron energy was set to be 1 keV. Argon gas was used to test the performance of this ion source (Ar^+ 95%, the rest are Ar^{n+}, n = 2–4) [36], the inlet argon gas pressure was 800 mbar and the extractor potential was −1550 V.

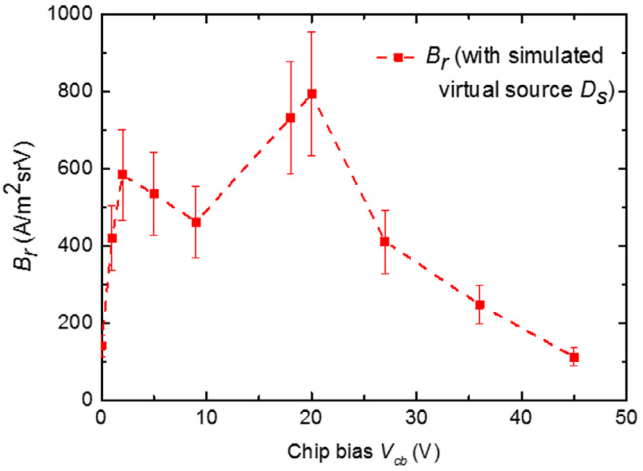

Fig. 6. Reduced brightness B_r as a function of chip bias V_{cb}.

The virtual ion source size was calculated by tracing the ray back from the angular aperture plane via beam optics simulation software Lorentz – 2EM [24,37]. The virtual source diameters D_s of full width 50% (FW50, the width that includes 50% of beam current) were obtained to calculate the beam reduced brightness, as shown in Fig. 6. The virtual source size is usually smaller than the physical source size and the maximum reduced brightness obtained is ~800 A/(m^{2}srV) with a chip bias of V_{cb} = 20 V. Here a total argon current of 200 pA was measured after extractor, with a 53 pA peak axial beam current collimated by angular aperture. This chip bias corresponds to an electric field of 8×10^6 A/m inside the ionization chamber, which is very close to the simulated condition (1×10^7 A/m). The observed low brightness of this prototype NAIS originates from the low reduced brightness of the electron injector (~900 A/(m^{2}srV)), low input gas pressure (800 mbar), large double-aperture size (1.3 μm), thick membranes (1 μm), and large spacer (500 nm). Also, the misalignment between NAIS and extractor contributes to the degradation of reduced brightness. Due to the relatively large chip bias, a larger energy spread is expected in the present experiment. We are working on improving the reduced brightness of NAIS beam by optimizing all of the above-mentioned parameters.

4. Conclusion

In this work, different configurations of NAIS have been examined through simulations and experiment. Our simulations indicate that the axial gas distribution is a crucial parameter to be considered in designing a chip which can confine the ionization and achieve low energy spread. The large double-aperture opening causes higher energy spread. Our calculations suggest that a high brightness proton beam can be obtained by employing 100 nm thick membranes having a 100 nm thick spacer with a 100 nm double-aperture configuration. This configuration can deliver proton beam with a reduced brightness of 10^6 A/(m^{2}srV), with less than 1 eV energy spread. To prevent the clogging of the double-aperture the injected electron beam diameter has to be kept smaller than the double-aperture.

The performance of the prototype NAIS [24] has been improved and reduced brightness of 800 A/(m^{2}srV) has been obtained. The potential beam brightness of NAIS is much higher than the experimental brightness value reported here. This discrepancy is caused by current experimental chip geometry and the low SEM electron beam brightness (~900 A/(m^{2}srV)). To improve this prototype NAIS, a newer design based on optimal simulation result is currently under development.

Acknowledgements

We thank the advice from Dr. C. W. Hagen and Dr. P. Kruit from CPO-TUD. We also thank Dr. S.K. Vajandar from our group for helpful discussion. We acknowledge the support from NRF Singapore (No. WBS R-263-000-B69-281) and thank the Centre for Advanced 2D Materials, NUS Singapore for the usage of their facilities.

References

[1] J.A. van Kan, A.A. Bettiol, F. Watt, Proton beam writing of three-dimensional nanostructures in hydrogen silsesquioxane, Nano Lett. 6 (2006) 579–582.
[2] F. Watt, M.B. Breese, A.A. Bettiol, J.A. van Kan, Proton beam writing, Mater. Today 10 (2007) 20–29.
[3] Y. Yao, M.W. van Mourik, P.S. Raman, J.A. van Kan, Improved beam spot measurements in the 2nd generation proton beam writing system, Nucl. Instrum. Methods Phys. Res., Sect. B 306 (2013) 265–270.
[4] Y. Wang, P. Malar, J.A. van Kan, Resist evaluation for proton beam writing, Ni mold fabrication and nano-replication, Microsyst. Technol. 20 (2014) 2079–2088.
[5] J. Simčič, P. Pelicon, Z. Rupnik, M. Mihelič, A. Razpet, D. Jenko, M. Maček, 3D micromachining of SU-8 polymer with proton microbeam, Nucl. Instrum. Methods Phys. Res., Sect. B 241 (2005) 479–485.
[6] V. Auzelyte, M. Elfman, P. Kristiansson, C. Nilsson, J. Pallon, N.A. Marrero, M. Wegdén, Exposure parameters for MeV proton beam writing on SU-8, Microelectron. Eng. 83 (2006) 2015–2020.
[7] P. Mistry, I. Gomez-Morilla, G. Grime, R. Webb, C. Jeynes, R. Gwilliam, A. Cansell, M. Merchant, K. Kirkby, Proton beam lithography at the University of Surrey's Ion Beam Centre, Nucl. Instrum. Methods Phys. Res., Sect. B 242 (2006) 387–389.
[8] F. Menzel, D. Spemann, S. Petriconi, J. Lenzner, T. Butz, Proton beam writing of submicrometer structures at LIPSION, Nucl. Instrum. Methods Phys. Res., Sect. B 260 (2007) 419–425.
[9] M. Abraham, I. Gomez-Morilla, M. Marsh, G. Grime, Proton induced structuring of a photostructurable glass, in: MRS Proceedings, Cambridge Univ Press, 2002, pp. H2. 8.
[10] I. Rajta, I. Gomez-Morilla, M. Abraham, A. Kiss, Proton beam micromachining on PMMA, Foturan and CR-39 materials, Nucl. Instrum. Methods Phys. Res., Sect. B 210 (2003) 260–265.
[11] J.A. van Kan, A.A. Bettiol, K. Ansari, E.J. Teo, T. Sum, F. Watt, Proton beam writing: a progress review, Int. J. Nanotechnol. 1 (2004) 464–479.
[12] C. Udalagama, A.A. Bettiol, F. Watt, Stochastic spatial energy deposition profiles for MeV protons and keV electrons, Phys. Rev. B 80 (2009) 224107.
[13] P. Mistry, I. Gomez-Morilla, G.W. Grime, R.P. Webb, R. Gwilliam, A. Cansell, M. Merchant, K.J. Kirkby, E.J. Teo, M.B.H. Breese, A.A. Bettiol, B. D.J., F. Watt, New developments in the applications of proton beam writing, Nucl. Instrum. Methods Phys. Res., Sect. B 237 (2005) 188–192.
[14] Y. Yao, P.S. Raman, J.A. van Kan, Orthogonal and fine lithographic structures attained from the next generation proton beam writing facility, Microsyst. Technol. 20 (2014) 2065–2069.
[15] Y. Yao, J.A. van Kan, Automatic beam focusing in the 2nd generation PBW line at sub-10nm line resolution, Nucl. Instrum. Methods Phys. Res., Sect. B 348 (2015) 203–208.
[16] C. Moak, H. Reese, W. Good, Design and operation of a radio-frequency ion source for particle accelerators, Nucleonics 9 (1951) 18–23.
[17] J.A. van Kan, P. Malar, A.B. De Vera, The second generation Singapore high resolution proton beam writing facility, Rev. Sci. Instrum. 83 (2012) 02B902.
[18] K.A. Twedt, L. Chen, J.J. McClelland, Scanning ion microscopy with low energy lithium ions, Ultramicroscopy 142 (2014) 24–31.
[19] B. Knuffman, A. Steele, J. McClelland, Cold atomic beam ion source for focused ion beam applications, J. Appl. Phys. 114 (2013) 044303.
[20] J.J. McClelland, A.V. Steele, B. Knuffman, K.A. Twedt, A. Schwarzkopf, T.M. Wilson, Bright focused ion beam sources based on laser-cooled atoms, Appl. Phys. Rev. 3 (2016) 011302.
[21] D.S. Jun, V.G. Kutchoukov, P. Kruit, Ion beams in SEM: an experiment towards a high brightness low energy spread electron impact gas ion source, J. Vac. Sci. Technol., B 29 (2011) 06F603.
[22] D. Jun, V. Kutchoukov, C. Heerkens, P. Kruit, Design and fabrication of a miniaturized gas ionization chamber for production of high quality ion beams, Microelectron. Eng. 97 (2012) 134–137.
[23] N. Liu, P.S. Raman, X. Xu, H.M. Tan, A. Khursheed, J.A. van Kan, Development of ion sources: towards high brightness for proton beam writing applications, Nucl. Instrum. Methods Phys. Res., Sect. B 348 (2015) 23–28.
[24] N. Liu, X. Xu, R. Pang, P.S. Raman, A. Khursheed, J.A. van Kan, Brightness measurement of an electron impact gas ion source for proton beam writing applications, Rev. Sci. Instrum. 87 (2016) 02A903.
[25] COMSOL Inc. COMSOL Multiphysics®. https://www.comsol.com/.
[26] Los Alamos National Laboratory, Accelerator Code Group. Poisson Superfish. http://laacg.lanl.gov/.
[27] Pulsar Physics. General Particle Tracer (GPT) package. http://www.pulsar.nl/gpt/.

[28] M. Bronsgeest, J. Barth, L. Swanson, P. Kruit, Probe current, probe size, and the practical brightness for probe forming systems, J. Vac. Sci. Technol., B 26 (2008) 949–955.
[29] J. Orloff, Handbook of Charged Particle Optics, CRC Press, 2008.
[30] C. Brau, What brightness means, The Physics and Applications of High Brightness Electron Beams, 1 (2003) 20–27.
[31] C.D. Child, Discharge from hot CaO, Phys. Rev. (Series I) 32 (1911) 492.
[32] I. Langmuir, The effect of space charge and initial velocities on the potential distribution and thermionic current between parallel plane electrodes, Phys. Rev. 21 (1923) 419.
[33] Y. Lau, Simple theory for the two-dimensional Child-Langmuir law, Phys. Rev. Lett. 87 (2001) 278301.
[34] L. Reimer, Scanning Electron Microscopy: Physics of Image Formation and Microanalysis, IOP Publishing, 2000.
[35] M. Breese, D. Jamieson, P. King, Materials Analysis with a Nuclear Microprobe, Wiley, New York, 1996.
[36] R. Rejoub, B. Lindsay, R. Stebbings, Determination of the absolute partial and total cross sections for electron-impact ionization of the rare gases, Phys. Rev. A 65 (2002) 042713.
[37] Integrated Engineering Software, Inc. Lorentz – 2EM (version 8.0). https://www.integratedsoft.com/.